ROYAL SOCIETY OF CHEMISTRY

Molecular BioSystems

High resolution metabolomics technology reveals widespread pathway changes of alcoholic liver disease

High resolution metabolomics technology reveals widespread pathway changes of alcoholic liver disease

Aihua Zhang[1,2‡], Guangli Yan[1,2‡], Xiaohang Zhou[1,2], Yangyang Wang[1,2], Ying Han[1,2], Yu Guan[1,2], Hui Sun[1,3]*, Xijun Wang[1,2]*

[1] National TCM Key Laboratory of Serum Pharmacochemistry, Laboratory of Metabolomics, Heilongjiang University of Chinese Medicine, Heping Road 24, Harbin 150040, China.

[2] Research Center of Chinmedomics, Heilongjiang University of Chinese Medicine, Heping Road 24, Harbin 150040, China.

[3] Department of Pharmaceutical Analysis, School of Pharmacy, Heilongjiang University of Chinese Medicine, Heping Road, Harbin, China.

Address correspondence to:

Prof. Xijun Wang

National TCM Key Laboratory of Serum Pharmacochemistry, Laboratory of Metabolomics, Research Center of Chinmedomics, Heilongjiang University of Chinese Medicine, Heping Road, Harbin, China. Tel. & Fax +86-451-82193039 Email: wangxijunomics@126.com

‡These authors contributed equally to this work.

Abstract:

Alcoholic liver disease (ALD) is a significant cause of death and morbidity. However little is known regarding the widespread pathway changes of ALD disorder. This study utilized metabolomic profiling to examining the pathogenic mechanisms of ALD based on rat model. A total 21 metabolites with significant changes were identified, involved several key metabolic pathways such as pentose and glucuronate interconversions, starch and sucrose metabolism, cysteine and methionine metabolism. Furthermore, the differential proteins corresponding alterations in metabolism across the metabolic network were identified using iTRAQ-based quantitative proteomics analysis. The proteins appear to be involved in protein binding, metabolism, immune response, and signal conduction. Interestingly, integrated omics profiling firstly reveals that p53 and Fc epsilon RI signaling pathways were closely related with ALD. Our study indicates that most of these proteins were found to play a pivotal role in the regulation of multiple metabolism pathways. Collectively, the current study provides insights into the molecular mechanisms of ALD from widespread pathway changes.

Introduction

Alcohol has been a part of human culture since the beginning of recorded history. Problems associated with excess alcohol consumption include social issues, increased accidents, chronic health problems and mortality [1]. Alcohol related morbidity in developed countries is second only to tobacco use and is responsible for 2.5 million deaths globally each year, and costs 1% of the GDP of middle to high income countries [2]. Alcohol misuse is a major public health problem in the worldwide and accounts for elevated social and economic costs. Alcoholic liver disease (ALD) is a common complication of alcohol misuse. Detection of ALD at an early stage could provide opportunities for more optimal management. The biomarkers including the erythrocyte mean cell volume, c-glutamyltransferase and carbohydrate-deficient transferring provide an objective measure of alcohol consumption, can assist in the detection of at-risk drinking [3]. Clearly, there is a need for more effective and definitive treatment options in order to improve prognosis and outcome of patients with severe ALD. Fortunately, integrated omics technology has been used to explore the particular metabolites, potentially diagnostic and prognostic biomarkers for deep understanding the essence of diseases [4-6].

At the end of the 20th century, genomics wrote out the 'script of life'; proteomics decoded the script; and metabolomics came into bloom [7]. These 'omics' quickly became the thrust of life sciences, pushing the discipline to new high. At present, numerous studies have discovered potential markers of disease using proteomics [8]. Isobaric tags for relative and absolute quantitation (iTRAQ), as a quantitative method, is a common tool in proteomics and has been extensively used for biomarker discovery in various disease contexts [9]. Metabolomics is the endpoints of genotype functions and biochemical phenotype in body, are linked closely to functions alteration in body, and incorporates a 'top-down' strategy to reflect the terminal symptoms of a whole system [10]. Recent advances have suggested that metabolite profiles will improve understanding the disease mechanisms [11-17]. Gobal metabolomic profiling with alcoholic fibrosis has proceeded very slowly, and changes in the serum proteomes of ALD are rarely reported. There is an urgent need for the discovery of novel molecular signatures to understand the underlying biological basis for ALD. However, to date there are few works aimed at gaining deeper insights into ALD through integrated metabolomics approach. Therefore, unlike other studies, this study was to devise the systematically integrated omics approach to focus and identify widespread pathway changes of ALD in rats.

Materials and Methods

Reagents.

HPLC grade acetonitrile was obtained from Merck (Darmstadt, Germany); methanol (HPLC grade) was purchased from Fisher Scientific Corporation (Loughborough, UK); water was produced by a Milli-Q Ultra-pure water system (Millipore, Billerica, USA); formic acid was obtained from Honeywell Company (Morristown, New Jersey, USA); leucine enkephalin was purchased from Sigma-Aldrich (St. Louis, MO, USA). iTRAQ reagent multi-plex kit,

containing the iTRAQ reagents, was bought commercially (Applied Biosystems, Foster City, CA, USA). The assay kits for alanine aminotransferase (ALT), aspartate amino transferase (AST), alkaline phosphatase (ALP), triglycerides (TG), total bilirubin (T-BIL), total protein (TP), albumin (ALB), total cholesterol (CHOL), hyaluronic acid (HA), laminin (LN), procollagen Iii (PIIINP), and collagen IV (CIV) were purchased from the Nanjing Jiancheng Biotech Company (Nanjing, China).

Animals.

Male Wistar rats were maintained in a specific pathogen-free environment. The animals were allowed to acclimatize in metabolic cages for 1 week prior to treatment. The animals were randomly assigned to 4 groups of 8 rats each as follows: control, 7w, 11w and 12w groups. The rats in the model group were orally administrated at a dose of 0.8ml/100g mixture (6g/kg alcohol liquor) and high-fat diet (high fat emulsion (10ml/kg)) for 12 consecutive weeks. The alcohol-fed model rats were fed ad libitum. Rats were sacrificed by an intraperitoneal injection of 1% pentobarbital sodium (0.15 ml/100 g body weight) at four time points: 4, 7, 11 and 12 weeks after initiation of injection. Livers were collected and washed three times with saline water. Each liver was cut into two pieces. The small piece was immediately fixed in buffered formalin for pathological staining. We collected plasma samples in heparinized tubes, kept them on ice for 1 h and centrifuged them at 5,000rpm for 20 min at 4°C, flash frozen in liquid nitrogen and stored at -80°C until the liver function tests and proteomics analyses were performed. Urine was collected daily (at 8:00 a.m.) from the metabolic cages at ambient temperature throughout the entire procedure and centrifuged at 10,000 rpm at 4°C for 5 min to remove any solid debris; the supernatants were then stored frozen at -80°C for subsequent metabolomic analysis. The study was approved by the Ethical Committee of Heilongjiang University of Chinese Medicine and was conducted according to the principles expressed in the Declaration of Helsinki.

Liver histology and biochemical assay

We quantified the levels of ALT, AST, ALP, TG, T-BIL, TP, ALB, CHOL, HA, LN, PCIIINP, CIV activities using assay kits according to the manufacturer's instructions. Liver samples from each rat were fixed in 10 % neutral buffered formaldehyde solution, embedded in paraffin, stained with hematoxylin-eosin (HE) and Masson trichrome collagen stain and then examined under an optical microscope.

Metabolomics analysis

Preparation of urine Samples Thawed urine samples were collected via centrifugation at 13,000 rpm for 10 minutes at 4∘C, and then filtered through a 0.22 μm syringe filter, 3 μL of the supernatant were injected into the UPLC/MS.

Chromatographic condition Urine metabolite profiling was performed using a Waters ACQUITY UPLC system (Waters Corporation, Milford, MA). The chromatographic separation was conducted on an Acquity HSS T3 column (100 mm x 2.1 mm, 1.8 μm). The column oven temperature was set to 45°C, injection volume at 3 μL and flow-rate at 0.4 ml/min without a split. The mobile phase consisted of phase A (acetonitrile containing 0.1% formic acid) and

phase B (water with 0.1% formic acid). The gradient was as follows: 0–2.5 min, 99–89% B; 2.5–4.5 min, 89–79% B; 4.5–7.0 min, 79–60% B; 7.0–7.5 min, 60-50% B; 7.5–10 min, 50–1% B; 10–12 min, 1% B; 12–12.5 min, 1–99% B; 12.5–15 min, 99% B.

Accurate mass time-of-flight mass spectrometry A Waters Micromass Q-TOF micro Synapt High Definition Mass Spectrometer (Synapt HDMS, Waters, Manchester, U.K.) equipped with electrospray ionization in positive and negative modes. MS/MS spectra were acquired as two separate positive ion (ESI+) and negative ion (ESI-) polarity runs for each sample. The following parameters were employed: ESI+: source temperature at 110 ◦C; capillary voltage was set at 3kv; cone voltage at 25 V; extraction cone voltage 3.0 V; the desolvation temperature was set at 300◦C; cone gas flow 50 L/h; desolvation gas flow 500 L/h; ESI-: source temperature at 110 ◦C; capillary voltage was set at 3kv; cone voltage at 30 V; extraction cone voltage 2.5V; the desolvation temperature was set at 300◦C; Cone gas flow 50 L/h; desolvation gas flow 400 L/h. Nitrogen was used as the drying gas, the desolvation gas flow rate was set at 500 L/h, and cone gas flow was maintained at 50 L/h. Collision energy was set at 35 eV in MS/MS mode for identification of potential metabolites. All the data were acquired using an independent reference lock mass (Leucine enkephalin) via the LockSpray[TM] interface to ensure accuracy and reproducibility during the MS analysis. Centroid data were collected at a rate of 1 MS spectrum per second from 100 to 1000 m/z with a scan time of 0.2 s, an inter-scan delay of 0.1 s, and a lock spray frequency of 10 s.

Multivariate statistical analysis The ion intensities for each peak were normalized within each sample, and then were introduced to EZinfo 2.0 software for principal components analysis (PCA), partial least-squared discriminant analysis (PLS-DA), orthogonal partial least-squared discriminant analysis (OPLS-DA) analysis. EZinfo 2.0 analysis software was used to extract molecular features in each of sample. VIP-plot which was constructed from the OPLS and was carried out to select distinct variables as potential biomarkers which were chosen based on their contribution to the variation and correlation within the data set. The ions furthest away from the origin in the VIP-plot may be therefore regarded as the differentiating metabolites. Student's t-test was performed to identify features with differential abundances across groups.

Metabolite identification Exact MS data from redundant m/z peaks were first used to help confirm the metabolite molecular mass. The candidate biomarkers were annotated based on retention behavior, mass assignment, and online database query. The accurate mass and structure information of candidate metabolites were matched with those of metabolites obtained from HMDB, METLIN, and Lipid Maps. The mass tolerance between the measured m/z values and the exact mass of the components of interest was set to within 5 mDa. Pathway analysis was performed using MetaboAnalyst tool.

iTRAQ-based quantitative proteomic analysis

Sample preparation and protein extraction. Plasma was fractionated with ProteinMiner Protein Enrichment Small-Capacity kit (Bio-Rad Laboratories, Hercules, CA, USA). Protein solutions were reduced for 1 h at 56˚C with

10 mM dithiothreitol and were cysteine blocked with 55 mM iodoacetamide at room temperature for 10 min. Each sample was precipitated with four times the volume of cold acetone.

Protein digestion and peptide tagging. Protein solutions were digested for 24 h with 10 μg L-1-(4-tosylamido)-2-phenylethyl tosylphenylalanyl chloromethyl ketone treated trypsin. Each peptide solution was labeled for 3 h at room temperature using an iTRAQ reagent (Applied Biosystems, Foster City, CA, USA). The reaction was terminated by adding MilliQ water, and the samples were labeled with tagged iTRAQ reagents.

Nano LC with tandem mass spectrometry. Nanoflow electrospray ionization tandem mass spectrometric analysis of peptide samples was carried out using Thermo fisher Q-Exactive (Thermo Scientific, Bremen, Germany) interfaced with Agilent's 1200 Series nanoflow LC system. The chromatographic capillary columns used were packed with Magic C18 (particle size 5 um, 100um x 150mm, Michrom Bioresources, CA, USA). The peptides were eluted using a linear gradient (0.01-50 min, 0% B; 50–51 min, 0–5% B; 51–71 min, 5–30% B; 71–76 min, 30-50% B; 76–81 min, 50% B; 81–86 min, 50-100% B; 86–96 min, 100% B.) over 96 min.

Protein identification and quantitative analysis. Peptides were quantified using the centroided reporter ion peak intensity. Intra-sample channels were normalized based on the median ratio for each channel across all proteins. Multiple isobaric tag samples were normalized by comparing the median protein ratios for the reference channel. Protein quantitative values were derived only from uniquely assigned peptides. The minimum quantitative value for each spectrum was calculated as the 5.0% of the highest peak. Protein quantitative ratios were calculated as the median of all peptide ratios. Fold-changes > 1.2 or and a two-tailed p-value <0.05 were set as cut-off values to designate significant protein expression changes. Independent component analysis (ICA) was performed to visualize the similarity of selected features between the test groups at different conditions.

Database screening and functional annotation Data were processed using BioTools software (Bruker Daltonics, Inc.). Gene Ontology (GO) functional classifications were analyzed with Blast2GO software, and GO enrichment analysis was performed to identify GO terms that were significantly enriched in DEP. Identified proteins were further analysed using STRING (http://string-db.org/) for protein-protein interactions. All statistical analyses were performed using the Student's t-test.

Results

Histopathology and Biochemical analysis

For histopathological analysis, liver samples were quickly obtained and fixed in a 10 % neutral buffered formaldehyde solution, embedded in paraffin and sectioned. Paraffin sections were stained with H&E for routine examination, followed by Masson staining for collagen. H&E staining and Masson's staining showed the presence of hepatic fibrosis, marked fatty degeneration, and collagen accumulation in the model group (**Fig.1A**). The HE staining showed that ALD was more severe in the 12W-treated group than in the 7W-treated group. Representative figures of

HE-stained sections of liver tissue from control group were evaluated as a normal histology. The liver lobules of the control group showed no pathological changes and the liver cells were normal. Compared with controls, liver cell steatosis was apparent in liver samples at 4W. Foci infiltration around fibrosis tissue can be seen. Large numbers of black and brown particles were deposited and accompanied with fibrosis tissue at 7W, and a similar pattern was evident at 12W. The collagen was shown to be green-colored in the Masson-stained section at 12W.

The extent of liver injury was assessed by measuring the enzymes of the liver in the mouse serum. As shown in the liver index, it was significantly different among the experimental groups. Liver index was decreased in rat groups compared to controls (**Fig.1B**). AST and ALT concentrations in serum were used as biochemical markers to evaluate hepatic injury. Serum activities of ALT and AST were found to be significantly increased in 12W-treated group when compared with control group ($p < 0.01$). The value of MDA in the serum was decreased ($p < 0.01$) in 12W-treated group, but the values of the activities of SOD in the liver tissue were increased ($p < 0.01$) compared to control group, and there was no significant change in either group at 4W. Both serum CHOL, TG, and the liver tissue Hyp, HA, LN, PCIIINP, CIV were markedly increased at 12W. The TP content in 12W-treated group were markedly decreased ($p < 0.01$), while the level of ALP, T-BA, TB, and r-GT were increased, compared with that of controls. A significant increase of the liver enzymes in the serum was occurred at 12W, and suggested that the degree of ALD. Consequently, combined with the histopathological manifestation results, we successfully established ALD in animal models at 12W.

Urine metabolomic profiles

Metabolomics involves studying the processes of all metabolites in diseased samples, thereby revealing disease-related metabolic pathways. The total ion chromatograms exhibited the ideal separation result under the optimized gradient elution procedure. Urine metabolomic profile for each sample consisted of approximately 8000 peaks. Low molecular mass metabolites could be separated well in the short time of 10 min. In order to better visualize the subtle similarities and differences among these complex data sets, multiple pattern recognition methods were employed to phenotype the urine metabolome of rats.

Multivariate statistical analysis Urine samples were analyzed in both positive and negative ionization modes with the UPLS/MS. Typically, the trajectory analysis of PCA score plots for the alcohol treatment in positive mode (**Fig.2A**) and negative ionization mode (**Fig.3A**) can really reflect a clear separation between the model and control groups. PCA plot of the model groups deviated from control group on 12W reached the maximum trend, the 4W to 7W gradually away to the normal state. The tracks of the metabolic profiles at different time points also clearly demonstrate the time dependent changes in the urine metabolites, which suggest that urinary biochemical perturbation significantly happened in model groups. To maximize the differences between the groups and determine the variables that contribute to discrimination, the OPLS-DA, a supervised pattern recognition method, was further employed for metabolic data (**Fig.2B** and **Fig.3B**).

Identification of metabolite candidates All chromatographic peaks were extracted for the discovery of metabolic biomarkers associated with ALD. For further analysis of feature ions, VIP-plot (**Fig.2C** and **Fig.3C**) from the OPLS and dendrogram analysis (**Fig.2D** and **Fig.3D**) of metabolite candidates were carried out to select distinct variables as potential biomarkers for distinguishing ALD from controls. From the corresponding VIP-plot, the ions furthest away from the origin may be therefore regarded as the differentiating metabolites. We generated VIP plots from the OPLS-DA with a threshold of 1.5 to identify the metabolites that significantly contribute to the clustering between groups. 21 differentially expressed small molecule metabolites considered to be strong contributors were distinguished from those of the healthy controls ($p < 0.05$, VIP>1.5, 8 ions in the positive mode and 13 ions in negative mode). Of note, it was found that, among them, 13 metabolites were upregulated and 8 metabolites were downregulated (**Table 1**). Histogram plots of **Fig.2E** and **2F** show relative signal intensities for 21 metabolites in control and ALD group.

Metabolic pathway and function analysis To gain insight into the metabolic mechanism of ALD, metabolic pathways of the significantly altered metabolites were analyzed using the ''pathway analysis'' module within the MetaboAnalyst software. We identified a total of seven distinct metabolic pathways that were significantly altered in the urine (**Table S1**) samples from model group. The detailed analysis of the most relevant pathways of ALD was performed by MetaboAnalyst's tool. A total of feature compounds in 7 pathways which were identified together are important for the host response to ALD (**Fig.S1A**). The predominant hits were pathways involved in pentose and glucuronate interconversions, starch and sucrose metabolism, cysteine and methionine metabolism, *etc*. The detailed construction of the perturbed pathways of pentose and glucuronate interconversions (**Fig.S1B**), starch and sucrose metabolism (**Fig.S1C**), cysteine and methionine metabolism (**Fig.S1D**) with higher score had yield satisfactory results (details in **Table S1**).

iTRAQ-proteomics analysis

ICA aggregates the set of proteins studied into one point per sample in the two-dimensional coordinate system spanned by the two most relevant independent components (**Fig.S2**). These trajectories reveal that the proteome profiles markedly change immediately after ALD. ICA can really reflect a clear separation between the 12W and control group.

Differentially expressed proteins To examine the difference in serum proteome between ALD rat models and controls, we conducted the analysis by iTRAQ. After trypsin digestion of total proteins, peptides from the model and control groups were labeled with 114 and 113, respectively. To identify the differentially expressed proteins (DEP), the relative protein expression values were compared between groups. These proteins could provide leads for potentially useful diagnostic and prognostic biomarkers for disease progression. The confidence value for each peptide was calculated based on agreement between the experimental and theoretical fragmentation patterns. Each protein was provided with a confidence score based on confidence scores of its constituent peptides with unique

spectral patterns. The threshold was set as < 0.83 and >1.2 for iTRAQ labeling, 85 proteins were identified as DEP between mouse models and controls at 12w time point. Of these, 33 were down-regulated (**Table S2**) and 52 were up-regulated in ALD model rat. To determine the proteins with abundance changes, a histogram was used to generate the number of proteins in different abundance ratio (**Fig.4**).

Gene ontology analysis We subjected the DEP to GO analysis and categorized them according to molecular function, biological processes and pathways. When we analyzed these proteins for molecular function (**Fig.S3**), we found that over 20% of proteins were grouped under "metabolism" such as macromolecule metabolic process, primary metabolic process and cellular metabolic process *etc*. The remaining DEP were grouped under "cellular process", "biological regulation", and "multicellular organismal process". Based on analysis of the cellular component, 51.13% of the DEP were annotated proteins. In the molecular function analysis of GO analysis, most DEP were associated with function of binding. Classification analysis of the biological processes with UniProt database and KEGG online tool (http://david.abcc.ncifcrf.gov/) showed the DEP are mainly involved in the processes of p53 signaling pathway, PPAR signaling pathway, fatty acid metabolism, TGF-beta signaling pathway, mTOR signaling pathway, cytokine-cytokine receptor interaction, purine metabolism, natural killer cell mediated cytotoxicity, neurotrophin signaling pathway, and Fc epsilon RI signaling pathway, respectively (**Table 2**). These data suggest that interruption of these pathways may provide a means to the development of molecularly targeted therapies for ALD. Interestingly, p53 signaling pathway (**Fig.S4**) including insulin-like growth factor-binding protein 3, insulin-like growth factor I, and Fc epsilon RI signaling pathway including Ig gamma-2C chain C region, RAC-gamma serine/threonine-protein kinase, was firstly reported in ALD. STRING analysis depicts known protein–protein interactions among genes of interest in overrepresented pathways (**Fig.5**). Tumor protein p53 acts as a tumor suppressor in many tumor types; induces growth arrest or apoptosis depending on the physiological circumstances and cell type. It is also involved in cell cycle regulation as a trans-activator that acts to negatively regulate cell division by controlling a set of genes required for this process.

Discussion

Alcohol consumption is one of the world's major risk factors for disease development. Ongoing studies show that alcohol consumption is associated with fatty liver disease in mammals. Recent advances in metabolomic technologies have enabled elucidate the effect of alcohol consumption on metabolism. Jaremek and co-workers have investigated the relation of alcohol intake and serum metabolite concentrations and identify potential biomarkers that could predict high levels of intake [18]. It suggests that alcohol affects mostly the sphingolipid, glycerophospholipid and ether lipid metabolism. Clugston and co-workers analyzed altered hepatic lipid metabolism in mice fed alcohol using a targeted lipidomic approach [19]. They found that chronic alcohol consumption is associated with increased hepatic free fatty acid levels and decreased fatty acyl-CoA levels associated with decreased mitochondrial fatty acid oxidation and

decreased fatty acyl-CoA synthesis, increased hepatic ceramide levels associated with higher levels of the precursor molecules sphingosine and sphinganine; and increased hepatic levels of the endocannabinoid anandamide associated with decreased expression of its catabolic enzyme fatty acid amide hydrolase. Kalhan et al. examined the plasma metabolomic profile in nonalcoholic fatty liver disease [20]. Their results suggested that markedly higher levels of glycocholate, taurocholate and glycochenodeoxycholate in subjects. A study showed that the expression of two proteins associated with alcoholic liver disease, peroxiredoxin 6 and aldehyde dehydrogenase 2, was down-regulated in ethanol fed rats [21]. As far as we are aware, no metabolomics-proteomics profiling analyses of ALD rats with alcohol consumption have yet been conducted.

In the present study, special attention was paid to the time points of the 1W and 12W which is closely associated with ALD, in the experimental animal model. The results showed that histopathology and biochemical results had significant differences between the controls and 12W. Through biochemical analysis combined with the histopathological results, we successfully established ALD in animal models at 12W. Additionally, alcoholic-induced ALD rat may be a useful model for determination of ALD. Metabolic changes are associated with a number of complex diseases. A panel of biomarkers to characterize disease could be useful for ALD diagnostics. In this paper, UPLC-MS combined with pattern recognition analysis approach were used to simplify and quicken the identification of the metabolites of ALD. UPLC-MS based metabolomics could be an advanced tool to help us find metabolites due to its capacity of processing large datasets, and classifying of sample groups, as well as its indiscriminative nature of metabolites. By using our metabolomics platform, PCA revealed a statistically significant separation between the ALD and control samples. OPLS model was built to find biomarker candidates of ALD and 21 statistically important variables with VIP>1.5 were defined, many are in various stages of progress at the ALD. Differential metabolites from the urine metabolome indicate the disrupted the pentose and glucuronate interconversions, starch and sucrose metabolism, cysteine and methionine metabolism pathways, *etc*, would be helpful for the understanding occurrence and development of ALD.

Proteomics, which measures mature proteins, could be used to closely observe biological functions in body [22]. Proteomics research is a potentially useful and effective tool for studying pathogenesis, establishing prognosis and determining treatment outcomes in a variety of diseases [23]. Though proteomics is widely performed, the changes in the serum proteomes of ALD are rarely reported due to the complicated mechanism of ALD, therefore this study was also to describe the changes in protein levels in ALD using iTRAQ proteomics. The authors hypothesized that this approach had the potential to ultimately be beneficial for the identification of proteins that were important in the progression of ALD. We constructed the mouse model of early stage of ALD using alcohol. Based on proteomics analysis, we investigated the proteomic changes and pathways leading to ALD by alcohol. For data analysis, we optimized the normalization of iTRAQ signals and quantified the expression of proteins identified. iTRAQ identified 85 different proteins that had ≥1.2-fold differences in expression level between the ALD with the controls. Finally, the

most significant pathway elucidated by bioinformatics methods was subsequently validated. Bioinformatics analysis of the DEP illustrated the enrichment of metabolism related processes, such as macromolecule metabolic process, primary metabolic process and cellular metabolic process *etc*. Studies have shown that p53 signaling pathway, PPAR signaling pathway, fatty acid metabolism, TGF-beta signaling pathway, mTOR signaling pathway, cytokine-cytokine receptor interaction, purine metabolism, natural killer cell mediated cytotoxicity, neurotrophin signaling pathway, and Fc epsilon RI signaling pathway are critical in the pathogenesis of ALD. Interestingly, p53 signaling pathway and Fc epsilon RI signaling pathway were firstly reported in ALD. This study helps to achieve a better understanding of the complexity of metabolic regulations of ALD, which may shed light on metabolism to ALD. GO analysis indicated that these proteins are involved in transport, biological regulation, cellular processes, immune response, and metabolic process. The DEP may be involved in the host response to ALD at the molecular level and may be potential diagnostic biomarkers for ALD. It also provides insights into the molecular basis for the use of PPAR signaling agonists, which has been advocated for treatment of ALD.

The findings yield a valuable tool that can engender new insights into the pathophysiology of ALD and advance the early diagnosis and monitor the progression of ALD, and showed that omics has the potential as a promising screening tool for exploring essence of ALD disease. In addition, future research will be directed to the biological interpretation: which pathways were involved in the biochemical changes associated with the onset, development and progression of ALD, and whether these changes are the same during onset and progression, or if different changes of biochemistry occur at the different stages of ALD. Thus, the findings presented contribute to a better understanding of the molecular signature of ALD and may provide the biological background to pharmacological interventions in the future.

Conclusions

ALD represents a significant cause of morbidity and mortality worldwide and constitute a problem of global public health importance. Therefore, it needs more reliable metabolism information for effective treatment. We successfully reproduced ALD in animal models from liver histology combined with biochemical results. Omics is a powerful approach for the comprehensive assessment of endogenous metabolites or proteins and attempts to systematically identify them from biological samples. In this study, the proteomics and metabolomics improves discrimination between ALD and control. Metabolomics approach coupled with multivariate statistical methods showed 21 altered metabolic biomarkers indicated that ALD could cause more severe disturbances in pentose and glucuronate interconversions, starch and sucrose metabolism, cysteine and methionine metabolism, *etc*. Using iTRAQ based proteomic methods, we identify 85 differentially expression proteins related to ALD, which might provide clues to clarify novel mechanisms underlying alcohol-induced ALD. Of these, 33 were down-regulated and 52 were up-regulated in ALD. Interestingly, integrated proteomic and metabolomic profiling reveal that p53 signaling

pathway and Fc epsilon RI signaling pathway were firstly found in ALD. These data suggest that interruption of these pathways may provide a means to the development of molecularly targeted therapies for ALD.

Additional Information:

The authors declare no competing financial interests.

References

1. George O, Sanders C, Freiling J, Grigoryan E, Vu S, Allen CD, Crawford E, Mandyam CD, Koob GF. Recruitment of medial prefrontal cortex neurons during alcohol withdrawal predicts cognitive impairment and excessive alcohol drinking. *Proc Natl Acad Sci U S A*, 2012, 109, 18156-18161.

2. Nasrallah NA, Clark JJ, Collins AL, Akers CA, Phillips PE, Bernstein IL. Risk preference following adolescent alcohol use is associated with corrupted encoding of costs but not rewards by mesolimbic dopamine. *Proc Natl Acad Sci U S A*, 2011, 108, 5466-5471.

3. Neumann T, Helander A, Dahl H, Holzmann T, Neuner B, Weiss-Gerlach E, Müller C, Spies C. Value of ethyl glucuronide in plasma as a biomarker for recent alcohol consumption in the emergency room. *Alcohol Alcohol*, 2008, 43, 431-435.

4. Sreekumar A, Poisson LM, Rajendiran TM, Khan AP, Cao Q, Yu J, Laxman B, Mehra R, Lonigro RJ, Li Y, Nyati MK, Ahsan A, Kalyana-Sundaram S, Han B, Cao X, Byun J, Omenn GS, Ghosh D, Pennathur S, Alexander DC, Berger A, Shuster JR, Wei JT, Varambally S, Beecher C, Chinnaiyan AM. Metabolomic profiles delineate potential role for sarcosine in prostate cancer progression. *Nature,* 2009, 457, 910-914.

5. Kuehnbaum NL, Gillen JB, Gibala MJ, Britz-McKibbin P. Personalized metabolomics for predicting glucose tolerance changes in sedentary women after high-intensity interval training. *Sci Rep,*2014, 4, 6166.

6. Wang X, Zhang A, Sun H. Power of metabolomics in diagnosis and biomarker discovery of hepatocellular carcinoma. *Hepatology,* 2013, 57, 2072-2077.

7. Sabidó E, Quehenberger O, Shen Q, Chang CY, Shah I, Armando AM, Andreyev A, Vitek O, Dennis EA,

Aebersold R. Targeted proteomics of the eicosanoid biosynthetic pathway completes an integrated genomics-proteomics-metabolomics picture of cellular metabolism. *Mol Cell Proteomics,* 2012, 11, M111.014746.

8. Kellie JF, Higgs RE, Ryder JW, Major A, Beach TG, Adler CH, Merchant K, Knierman MD. Quantitative measurement of intact alpha-synuclein proteoforms from post-mortem control and Parkinson's disease brain tissue by intact protein mass spectrometry. *Sci Rep*, 2014, 4, 5797.

9. Sun L, Bertke MM, Champion MM, Zhu G, Huber PW, Dovichi NJ. Quantitative proteomics of Xenopus laevis embryos: expression kinetics of nearly 4000 proteins during early development. *Sci Rep*,2014, 4, 4365.

10. Wang TJ, Larson MG, Vasan RS, Cheng S, Rhee EP, McCabe E, Lewis GD, Fox CS, Jacques PF, Fernandez C, O'Donnell CJ, Carr SA, Mootha VK, Florez JC, Souza A, Melander O, Clish CB, Gerszten RE. Metabolite profiles and the risk of developing diabetes. *Nat Med*, 2011, 17, 448-453.

11. Patti GJ, Yanes O, Shriver LP, Courade JP, Tautenhahn R, Manchester M, Siuzdak G. Metabolomics implicates altered sphingolipids in chronic pain of neuropathic origin. *Nat Chem Biol,* 2012, 8, 232-234.

12. Chen Y, Xu J, Zhang R, Shen G, Song Y, Sun J, He J, Zhan Q, Abliz Z. Assessment of data pre-processing methods for LC-MS/MS-based metabolomics of uterine cervix cancer. *Analyst.* 2013;138(9):2669-77

13. Pacchiarotta T, Derks RJ, Nevedomskaya E, van der Starre W, van Dissel J, Deelder A, Mayboroda OA. Exploratory analysis of urinary tract infection using a GC-APCI-MS platform. *Analyst.* 2015;140(8):2834-41.

14. Wang X, Zhang A, Han Y, Wang P, Sun H, Song G, Dong T, Yuan Y, Yuan X, Zhang M, Xie N, Zhang H, Dong H, Dong W. Urine metabolomics analysis for biomarker discovery and detection of jaundice syndrome in patients with liver disease. *Mol Cell Proteomics,* 2012,11, 370-380.

15. Nadal-Desbarats L, Aïdoud N, Emond P, Blasco H, Filipiak I, Sarda P, Bonnet-Brilhault F, Mavel S, Andres CR. Combined 1H-NMR and 1H-13C HSQC-NMR to improve urinary screening in autism spectrum disorders. *Analyst.* 2014;139(13):3460-3468.

16. Sun H, Zhang A, Yan G, Piao C, Li W, Sun C, Wu X, Li X, Chen Y, Wang X. Metabolomic analysis of key regulatory metabolites in hepatitis C virus-infected tree shrews. *Mol Cell Proteomics,* 2013,12, 710-719.

17. Zhang A, Sun H, Wang X. Urinary metabolic profiling of rat models revealed protective function of scoparone against alcohol induced hepatotoxicity. *Sci Rep* 2014, 4, 6768.

18. Jaremek M, Yu Z, Mangino M, Mittelstrass K, Prehn C, Singmann P, Xu T, Dahmen N, Weinberger KM, Suhre K, Peters A, Döring A, Hauner H, Adamski J, Illig T, Spector TD, Wang-Sattler R. Alcohol-induced metabolomic differences in humans. *Transl Psychiatry*, 2013, 3, e276.

19. Clugston RD, Jiang H, Lee MX, Piantedosi R, Yuen JJ, Ramakrishnan R, Lewis MJ, Gottesman ME, Huang LS, Goldberg IJ, Berk PD, Blaner WS. Altered hepatic lipid metabolism in C57BL/6 mice fed alcohol: a targeted lipidomic and gene expression study. *J Lipid Res*, 2011, 52, 2021-2031.

20. Kalhan SC, Guo L, Edmison J, Dasarathy S, McCullough AJ, Hanson RW, Milburn M. Plasma metabolomic

profile in nonalcoholic fatty liver disease. *Metabolism,* 2011, 60, 404-413.

21. Newton BW, Russell WK, Russell DH, Ramaiah SK, Jayaraman A. Liver proteome analysis in a rodent model of alcoholic steatosis. *J Proteome Res,* 2009, 8, 1663-1671.

22. Rhee HW, Zou P, Udeshi ND, Martell JD, Mootha VK, Carr SA, Ting AY. Proteomic mapping of mitochondria in living cells via spatially restricted enzymatic tagging. *Science,* 2013, 339, 1328-1331.

23. Wagner R, Li J, Kenar E, Kohlbacher O, Machicao F, Häring HU, Fritsche A, Xu G, Lehmann R. Clinical and non-targeted metabolomic profiling of homozygous carriers of Transcription Factor 7-like 2 variant rs7903146. *Sci Rep*, 2014, 4, 5296.
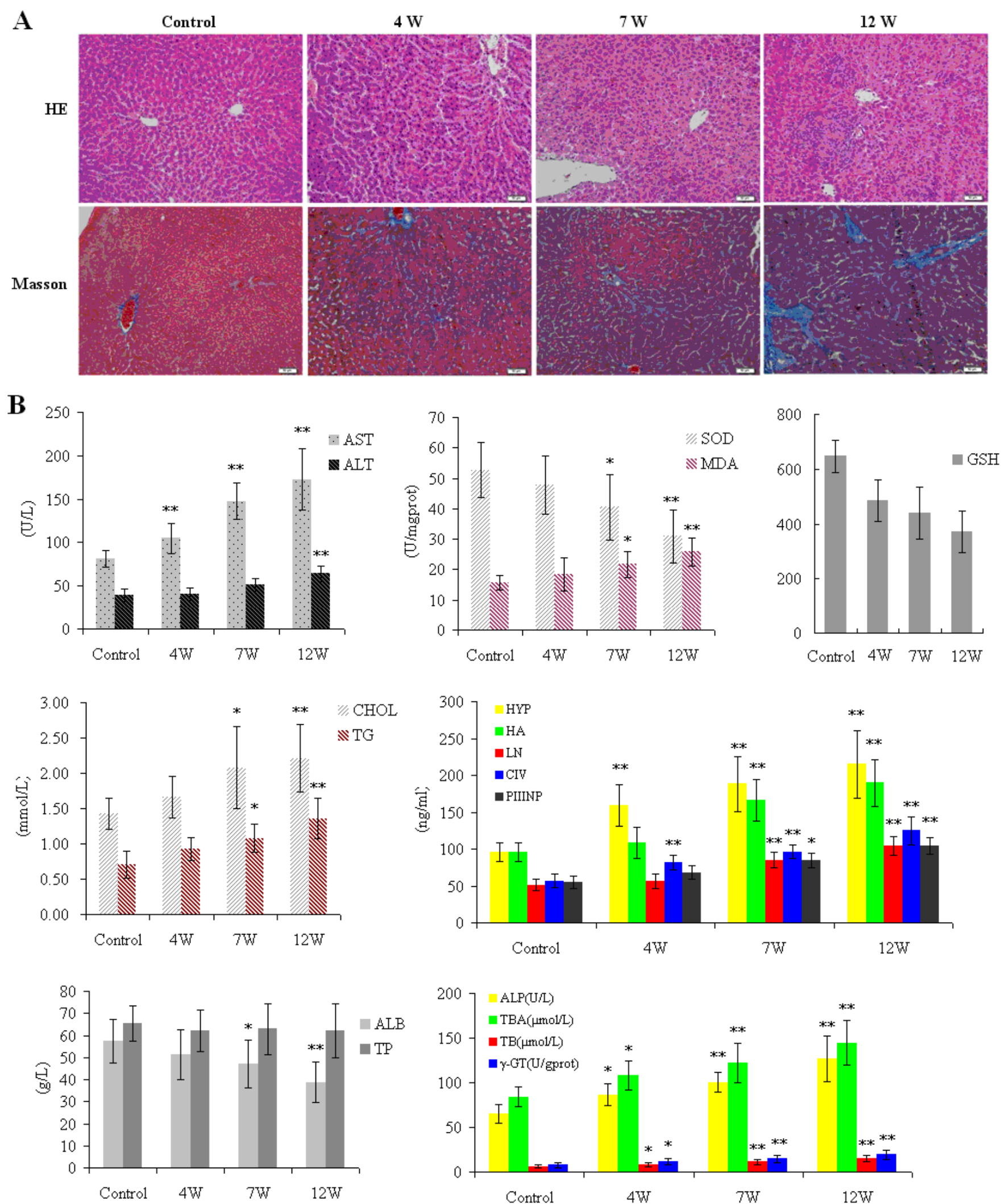
Fig.1 Representative photomicrographs of rat liver tissues with Hematoxylin and Eosin (200×) and Masson Staining

(200×) in the experimental rats (A). Liver tissue from model group showed disorderly hepatocyte cords, severe fatty

degeneration, spotty or focal necrosis and infiltration of inflammatory cells; hemorrhagic necrosis with foci of

lymphomonocytic infiltration around fibrosis tissue can be seen. Biochemical analysis (B). The extent of liver injury

was assessed by measuring the enzymes of the liver in the mouse serum. As shown in the liver index, serum activities

of ALT and AST were found to be significantly increased in 12W-treated group when compared with control group.

The value of MDA in the serum was decreased in 12W-treated group, but the values of the activities of SOD in the

liver tissue were increased compared to control group, and there was no significant change in either group at 4W. Both serum CHOL, TG, and the liver tissue Hyp, HA, LN, PCIIINP, CIV were markedly increased at 12W. The TP content in 12W-treated group were markedly decreased, while the level of ALP, T-BA, TB, and r-GT were increased, compared with that of controls. A significant increase of the liver enzymes in the serum was occurred at 12W. The values are expressed as mean± SD. * P<0.05 and ** P<0.01, vs. control group.
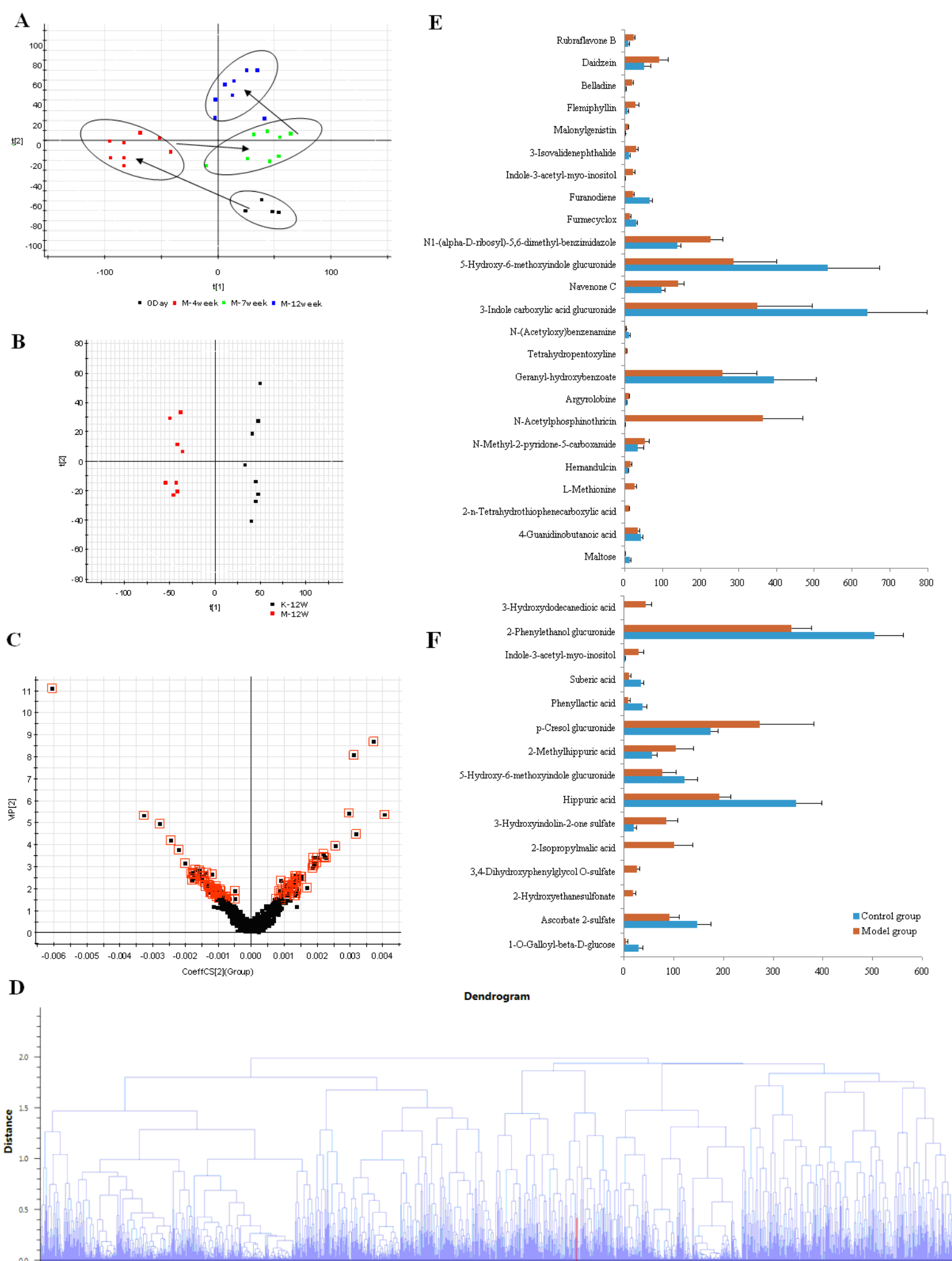
Fig.2 Metabolomic multivariate analysis of untargeted metabolomics data. Trajectory analysis of principal components analysis score plots of the alcoholic ALD at the continuous 12W in positive mode (A); partial least-squared discriminant analysis plot of ALD in positive mode (B); Panel C shows the VIP-score plots constructed from the supervised orthogonal partial least-squared discriminant analysis of urine. Ions with the highest abundance and correlation in model group with respect to the controls are present on the upper far right hand quadrant, whereas ions with the lowest abundance and correlation in the ALD with respect to the control group are residing in the lower far left hand quadrant. (D) Dendrogram analysis of metabolite candidates. Histogram plots show the relative signal intensities for marker metabolites for the control and model groups in positive mode (E) and negative mode (F).
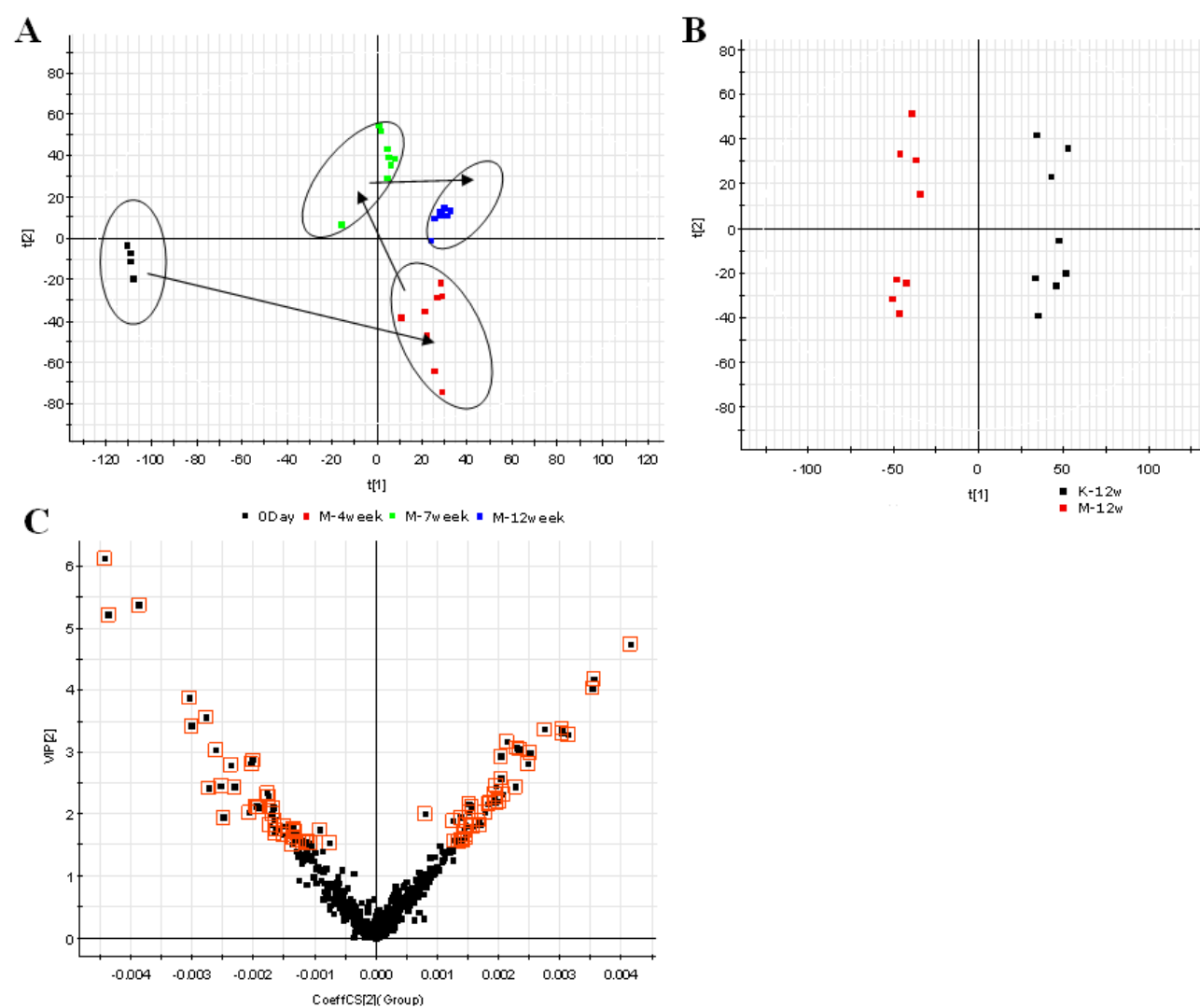
Fig.3 Metabolomic profiling of AFLD. Principal components analysis model results for ALD group in negative mode (A). Loading plot of partial least-squared discriminant analysis in positive mode (C). Panel C shows the combination of VIP-score plots constructed from the supervised orthogonal partial least-squared discriminant analysis of urine (ESI- mode).
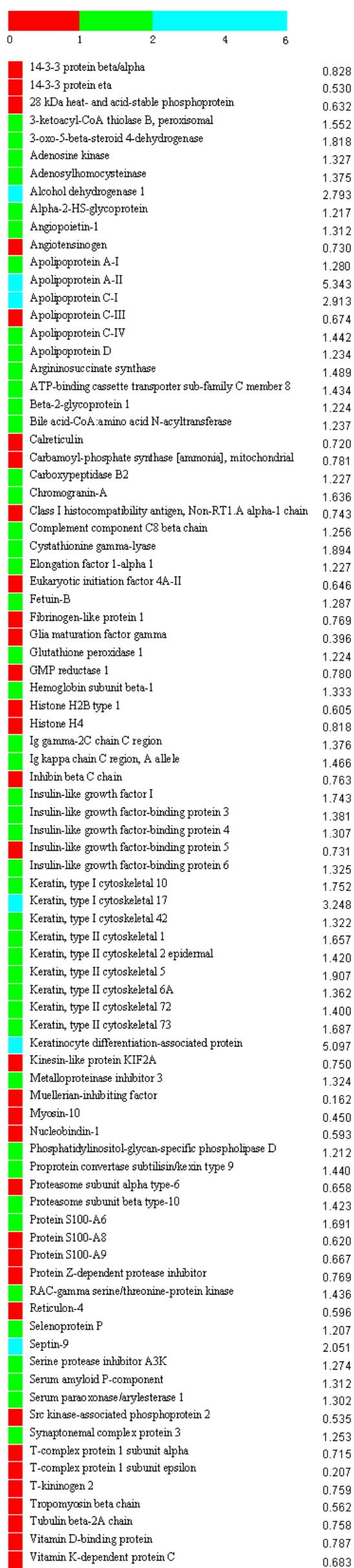
Fig.4 Heatmap for the differentially regulated proteins in biosamples.

Fig.5 STRING analysis depicting known protein–protein interactions among genes of interest in overrepresented pathways. Modes of action are shown in different colors. Differentially expressed proteins are represented as pill-shaped nodes, while proteins are shown as spheres. p53 signaling pathway (A) and Fc epsilon RI signaling pathway (B)

Table 1. Urinary biomarker candidates in alcoholic liver disease rat identified by UPLC/ESI-Q/TOF-MS.

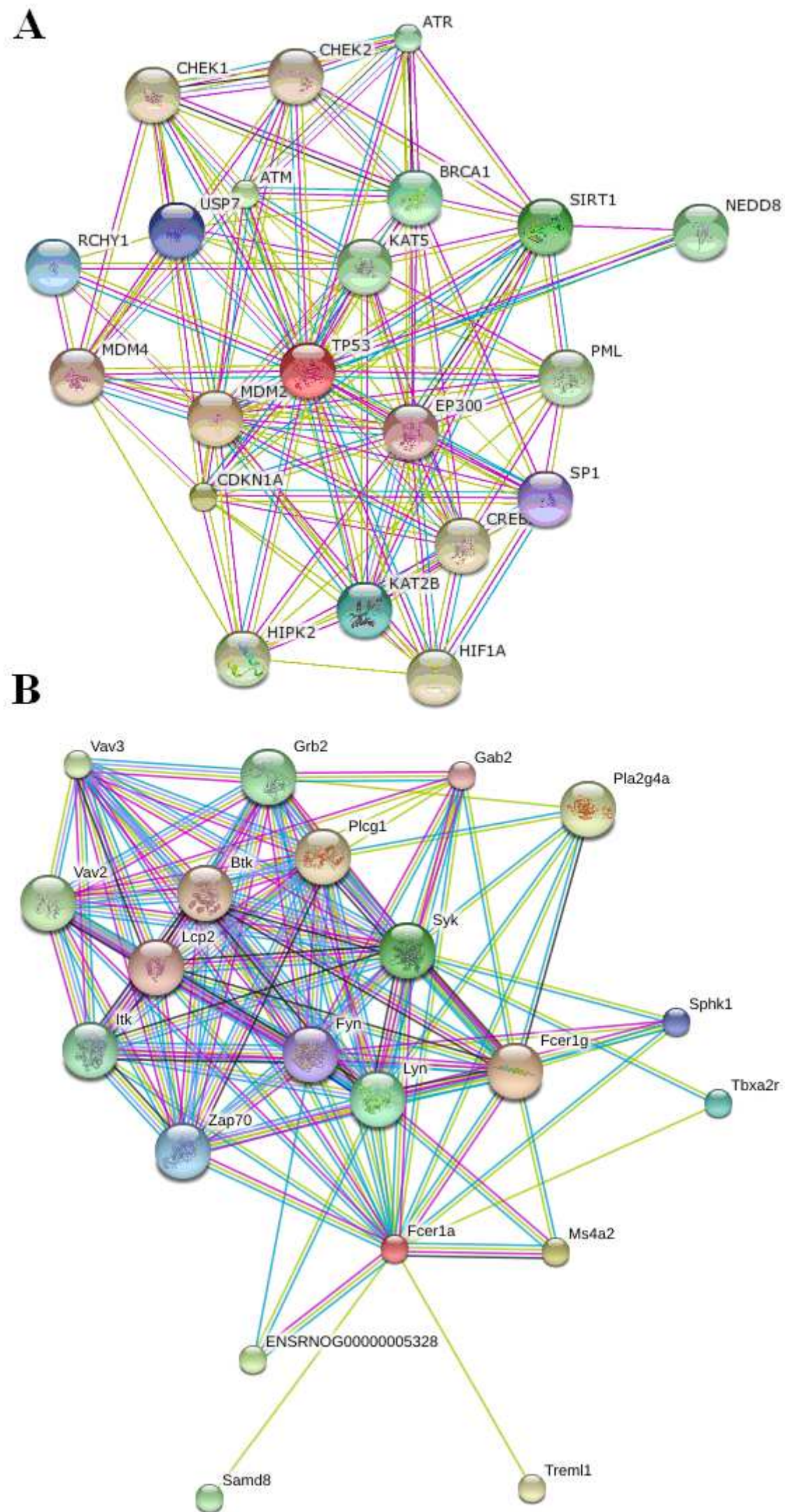| No.	Retention time/min	Ion form	Determined mass/Da	Calculated mass/Da	Error/mDa	Formula	Identity	VIP-Value	t-test /p-value	Trend
1	1.05	[M+H]$^+$	150.0581	150.0589	-0.8	$C_5H_{11}NO_2S$	L-Methionine	2.9	4.65E-08	↑
2	1.78	[M+H]$^+$	153.0647	153.0664	-1.7	$C_7H_8N_2O_2$	N-Methyl-2-pyridone-5-carboxamide	1.9	3.88E-02	↑
3	1.81	[M+H]$^+$	246.0547	246.0507	4.0	$C_7H_{14}NO_5P$	N-Acetylphosphinothricin	11.1	1.19E-07	↑
4	3.59	[M+H]$^+$	152.0698	152.0712	-1.4	$C_8H_9NO_2$	N-(Acetyloxy)benzenamine	1.5	1.03E-03	↓
5	4.03	[M+H]$^+$	338.0883	338.0876	0.7	$C_{15}H_{15}NO_8$	3-Indole carboxylic acid glucuronide	8.7	1.87E-03	↓
6	4.26	[M+H]$^+$	340.1020	340.1022	-0.2	$C_{15}H_{17}NO_8$	5-Hydroxy-6-methoxyindole glucuronide	8.1	1.46E-03	↓
7	4.61	[M+H]$^+$	279.1328	279.1345	-1.7	$C_{14}H_{18}N_2O_4$	N1-(alpha-D-ribosyl)-5,6-dimethyl-benzimidazole	5.3	6.08E-06	↑
8	5.91	[M+H]$^+$	338.1247	338.1240	0.7	$C_{16}H_{19}NO_7$	Indole-3-acetyl-myo-inositol	2.7	1.08E-07	↑
9	0.70	[M-H]$^-$	377.0752	377.0720	3.2	$C_{13}H_{16}O_{10}$	1-O-Galloyl-beta-D-glucose	2.1	6.19E-06	↓
10	0.87	[M-H]$^-$	124.9908	124.9909	-0.1	$C_2H_6O_4S$	2-Hydroxyethanesulfonate	1.8	4.51E-07	↑
11	0.89	[M-H]$^-$	295.0138	295.0124	1.4	$C_8H_{10}O_7S$	3,4-Dihydroxyphenylglycol O-sulfate	2.2	2.63E-08	↑
12	1.26	[M-H]$^-$	221.0656	221.0661	-0.5	$C_7H_{12}O_5$	2-Isopropylmalic acid	4.2	4.78E-06	↑
13	1.87	[M-H]$^-$	227.9975	227.9967	0.8	$C_8H_6NO_5S$	3-Hydroxyindolin-2-one sulfate	3.4	3.04E-06	↑
14*	3.61	[M-H]$^-$	178.0515	178.0504	1.1	$C_9H_9NO_3$	Hippuric acid	5.2	2.71E-06	↓
15	4.26	[M-H]$^-$	338.0865	338.0876	-1.1	$C_{15}H_{17}NO_8$	5-Hydroxy-6-methoxyindole glucuronide	2.4	5.408E-03	↓
16	4.28	[M-H]$^-$	192.0649	192.0661	-1.2	$C_{10}H_{11}NO_3$	2-Methylhippuric acid	2.6	3.11E-03	↑
17	5.10	[M-H]$^-$	283.0810	283.0818	-0.8	$C_{13}H_{16}O_7$	p-Cresol glucuronide	5.5	2.45E-06	↑
18	5.51	[M-H]$^-$	173.0815	173.0814	0.1	$C_8H_{14}O_4$	Suberic acid	2.0	4.17E-06	↓
19	5.91	[M-H]$^-$	336.1071	336.1083	-1.2	$C_{16}H_{19}NO_7$	Indole-3-acetyl-myo-inositol	2.2	3.2E-06	↑
20	6.77	[M-H]$^-$	297.0970	297.0974	-0.4	$C_{14}H_{18}O_7$	2-Phenylethanol glucuronide	5.4	1.08E-05	↓
21	8.01	[M-H]$^-$	291.1290	291.1287	0.3	$C_{12}H_{22}O_5$	3-Hydroxydodecanedioic acid	2.8	7.99E-08	↑

* detected metabolites in both positive and negative modes.

No.	Retention time/min	Ion form	Determined mass/Da	Calculated mass/Da	Error/mDa	Formula	Identity	VIP-Value	t-test /p-value	Trend
1	1.05	[M+H]$^+$	150.0581	150.0589	-0.8	$C_5H_{11}NO_2S$	L-Methionine	2.9	4.65E-08	↑
2	1.78	[M+H]$^+$	153.0647	153.0664	-1.7	$C_7H_8N_2O_2$	N-Methyl-2-pyridone-5-carboxamide	1.9	3.88E-02	↑
3	1.81	[M+H]$^+$	246.0547	246.0507	4.0	$C_7H_{14}NO_5P$	N-Acetylphosphinothricin	11.1	1.19E-07	↑
4	3.59	[M+H]$^+$	152.0698	152.0712	-1.4	$C_8H_9NO_2$	N-(Acetyloxy)benzenamine	1.5	1.03E-03	↓
5	4.03	[M+H]$^+$	338.0883	338.0876	0.7	$C_{15}H_{15}NO_8$	3-Indole carboxylic acid glucuronide	8.7	1.87E-03	↓
6	4.26	[M+H]$^+$	340.1020	340.1022	-0.2	$C_{15}H_{17}NO_8$	5-Hydroxy-6-methoxyindole glucuronide	8.1	1.46E-03	↓
7	4.61	[M+H]$^+$	279.1328	279.1345	-1.7	$C_{14}H_{18}N_2O_4$	N1-(alpha-D-ribosyl)-5,6-dimethyl-benzimidazole	5.3	6.08E-06	↑
8	5.91	[M+H]$^+$	338.1247	338.1240	0.7	$C_{16}H_{19}NO_7$	Indole-3-acetyl-myo-inositol	2.7	1.08E-07	↑
9	0.70	[M-H]$^-$	377.0752	377.0720	3.2	$C_{13}H_{16}O_{10}$	1-O-Galloyl-beta-D-glucose	2.1	6.19E-06	↓
10	0.87	[M-H]$^-$	124.9908	124.9909	-0.1	$C_2H_6O_4S$	2-Hydroxyethanesulfonate	1.8	4.51E-07	↑
11	0.89	[M-H]$^-$	295.0138	295.0124	1.4	$C_8H_{10}O_7S$	3,4-Dihydroxyphenylglycol O-sulfate	2.2	2.63E-08	↑
12	1.26	[M-H]$^-$	221.0656	221.0661	-0.5	$C_7H_{12}O_5$	2-Isopropylmalic acid	4.2	4.78E-06	↑
13	1.87	[M-H]$^-$	227.9975	227.9967	0.8	$C_8H_6NO_5S$	3-Hydroxyindolin-2-one sulfate	3.4	3.04E-06	↑

1

Table 2. List of the pathway associated with differentially expressed proteins in the iTRAQ experiments.

No.	Pathway	Pathway ID	Proteins
1	p53 signaling pathway	ko04115	P15473, P08025
2	PPAR signaling pathway	ko03320	P06759, P04639, P07871, P04638
3	Fatty acid metabolism	ko00071	P07871, P06757
4	TGF-beta signaling pathway	ko04350	P49000, Q9WUK5
5	mTOR signaling pathway	ko04150	Q63484, P08025
6	Cytokine-cytokine receptor interaction	ko04060	P49000, Q9WUK5
7	Purine metabolism	ko00230	Q9Z244, Q64640
8	Natural killer cell mediated cytotoxicity	ko04650	P15978, P20762
9	Neurotrophin signaling pathway	ko04722	P68511, P35213, Q63484
10	Fc epsilon RI signaling pathway	ko04664	P20762, Q63484